Proceedings of the 7th International Conference on Mechanics and Materials in Design
Albufeira/Portugal 11-15 June 2017. Editors J.F. Silva Gomes and S.A. Meguid.
Publ. INEGI/FEUP (2017)

PAPER REF: 6819

STOCHASTIC FATIGUE CALCULATIONS USING AN ACCELERATED 3-STEP MULTILINEAR KINEMATIC HARDENING MODEL OF SPHEROIDAL GRAPHITE IRON

Martin Dazer[1(*)], Peter Höller[1], Tobias Leopold[2], Bernd Bertsche[1]
[1]Institute of Machine Components (IMA), University of Stuttgart, Stuttgart, Germany
[2]Knorr-Bremse Systeme für Nutzfahrzeuge GmbH (KB-SFN GmbH), München, Germany
[(*)]*Email:* martin.dazer@ima.uni-stuttgart.de

ABSTRACT
Precise lifetime predictions are essential during product development to meet short development times. For this purpose, high-quality material models are required, which are able to represent the stress occurring in products with high accuracy. In this work, four different hardening models are presented which take into account different flow laws and hardening effects. According to (Dazer, 2016) many designs have to be calculated for the stochastic lifetime predictions. Therefore, evaluation criteria is also calculation time in addition to the accuracy of the approximation. The result is that the stress in the component can be described accurate with a 3-step transition from static to cyclic behavior.

Keywords: Kinematic hardening model, nonlinear hardening model, stochastic fatigue calculations, damage calculation

INTRODUCTION

Most products lifetime is tested with high loads in order to obtain results faster. In case of known accelerating factors these results allow lifetime predictions for field stress (Nelson, 2004). At high load levels, plasticizing is increasing, which influences the fatigue strength due to mechanic hardening or softening. To obtain precise lifetime predictions, simulation models must be able to describe these effects. According to the state of the art (Leutwein, 2007), mostly the purely cyclic behavior is regarded, which leads to inadequate results with cyclical hardening materials.

The elasticity of the material is initially over-estimated, leading to lower plastic strains and to high stresses in the simulation. In addition, stress relaxation and cyclic creeping occur under cyclic load resulting in a time dependent damage behavior (Haibach, 2006). First of all, different material models will be compared in terms of accuracy and computing time. For validation real data is gathered from a brake caliper of the KB-SfN GmbH, made of spheroidal graphite casting iron GJS 600-6 with an applied strain gauge. For the material data samples were taken from the strut of the brake caliper, see fig. 1.

To carry out the stochastic lifetime prediction according to (Dazer, 2016) the material model must be able to represent variance of material characteristics in very low computing time. Therefore a stochastic modeling of the material behavior of the best model is necessary. In order to validate the stochastic material model, lifetime tests were performed with different brake calipers.

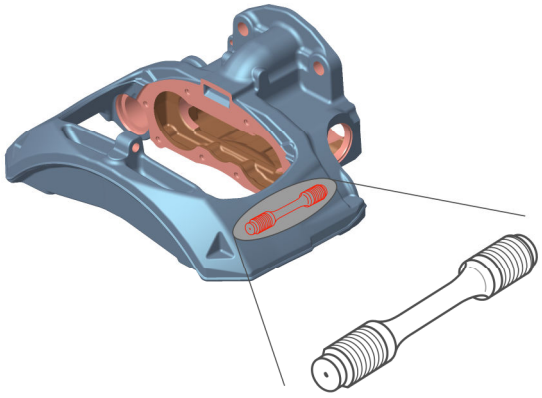

Fig. 1 Sample from the brake caliper

DEFINITION AND IMPLEMENTATION OF THE MATERIAL MODELS

Four models are presented and compared in terms of accuracy and calculation time.

- Model 1: cyclic behavior with multilinear kinematic hardening (mkh);
- Model 2: cyclic behavior with nonlinear kh Chaboche model (Lemaitre, 1990);
- Model 3: 3-step mkh;
- Model 4: 2-step mkh & cyclic behavior with nonlinear kinematic hardening.

Model 1 and 3 are based on the Ramberg-Osgood (RO) equation (Ramberg, 1943) with multilinear kinematic hardening behavior, see eq. 1.

$$\varepsilon_{a,t} = \frac{\sigma}{E} + \left(\frac{\sigma}{K}\right)^{1/n} \tag{1}$$

The flow surface remains constant during kinematic hardening. The flow criterion depends on the displacement of the flow surface (Miramontes, 1996). According to Prager rule (Prager, 1955), the Tensor X describes the current position of the flow surface. The yield strength R_e remains constant.

$$f(\sigma, X) = F(\sigma - X) - R_e \tag{2}$$

For the description of the stress-strain correlation, the hardening coefficient K and the hardening exponent n are required in addition to the young's modulus. For static cases, they are obtained from tensile tests and for cyclic cases from strain-controlled fatigue strength tests. Model 1 is using cyclically stable behavior from the first load step with a constant flow criterion and hardening rule and therefore represents state of the art. The 3-step hardening model 3 considers the transition from static to cyclic behavior. Thereto, the first load step is calculated with the static first load model n and K from tensile test. Casting materials often show a different material behavior when the load is released, which is described by the Bauschinger-Effect (Berns, 2013).

Consequently, the first load release is modeled with the load release behavior n' and K'. It is assumed that the material is already cyclically hardened with the beginning of the third load step, which is why cyclically stable behavior n'' and K'' is modeled from then on. Within a calculation step, the flow criterion remains constant. Between the calculation steps (transition from static to load release and from load release to cyclic data), a discrete change of the flow criterion is conducted. The Young's modulus increases by 20 GPa from static to cyclic

behavior, which is also considered in model 3. Table 1 and fig. 2 show the median values and the median stress-strain correlation of the modeled data. (Leutwein, 2007) used a similar procedure to determine the influence of autofrettage of cylinders with internal pressure loading.

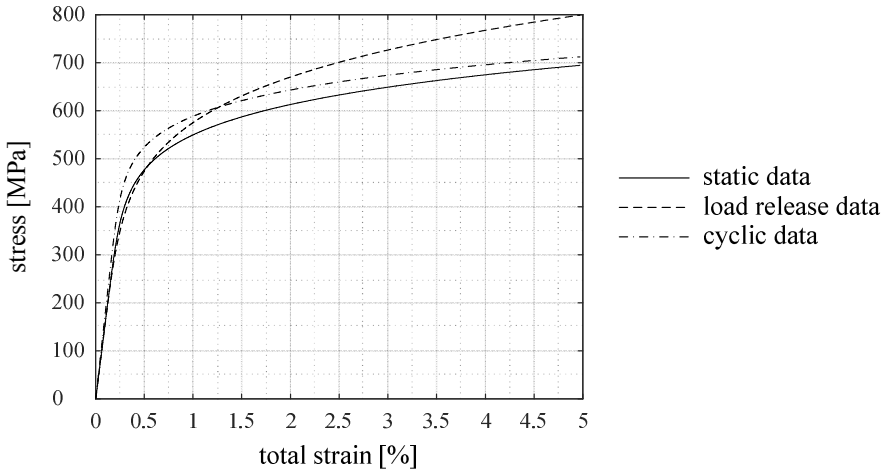

Fig. 2 - Stress-strain correlation of modeled material data

Table 1 - Median values of material data

	static data			**load release data**			**cyclic data**		
	K	*n*	*E* [GPa]	*K'*	*n'*	*E* [GPa]	*K''*	*n''*	*E* [GPa]
model 1	-	-	180	-	-	180	959	0,1	180
model 3	1000	0,5	160	1340	0,17	160	959	0,1	180

The integration into the FEM software Ansys is accomplished with 20 pairs of values of stress and plastic strain. For model 3, each load case is calculated with the corresponding material data. The elastic components are integrated separately with an isotropic behavior, which is defined by the Young's modulus and the Poisson's ratio. The yield strength is used for separation between elastic and elastic-plastic behavior, because theoretically the first plastic deformation in the component occurs at this point. Accordingly, the pairs of values have to begin at the yield strength and an associated plastic strain of $\varepsilon_{pl} = 0$. GJS600-6 is a material without a pronounced yield strength, why an approximate solution is used for the determination. If the deviation between the purely elastic ε_{el} and the elastic-plastic ε_t behavior exceeds the limit of $\Delta\varepsilon_{crit}$ = 0.07 % for the initial load or $\Delta\varepsilon_{crit}$ = 0.02 % for the first load release and the cyclic load, the approx. yield strength R_e' is defined at the corresponding stress of $\Delta\varepsilon_{crit}$, see eq. 3 and fig. 3. The limit value $\Delta\varepsilon_{crit}$ was empirically adjusted to the real data and tends to the conservative side to avoid too small plastic strains.

The stresses for the pairs of values are divided with a constant step size between approx. yield strength R_e' and tensile strength R_m. A conversion from technical to true values according to eq. 4 and eq. 5 is necessary (Zahavi, 1996), because in tests the change of cross section is not considered.

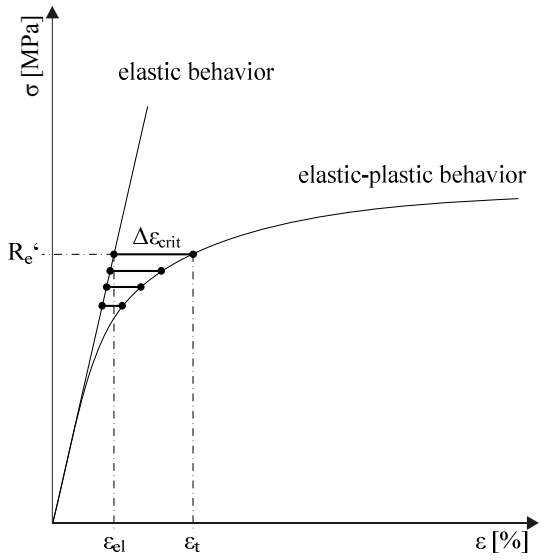

Fig. 3 - Numeric determination of approx. yield strength R_e‘

$$\Delta\varepsilon_{crit} = \varepsilon_t - \varepsilon_{el} = \left(\frac{\sigma_a}{E} + \left(\frac{\sigma_a}{K}\right)^{1/n}\right) - \frac{\sigma_a}{E} = \left(\frac{\sigma_a}{K}\right)^{1/n} \tag{3}$$

$$\sigma_{true} = \sigma(1 + \varepsilon_{tec}) \tag{4}$$

$$\varepsilon_{true} = \ln(1 + \varepsilon_{tec}) \tag{5}$$

Stresses result in:

$$\sigma = \sigma\left(1 + \frac{\sigma}{E}\right) + \left(\frac{\sigma}{K}\right)^{1/n} \tag{6}$$

The corresponding strains are calculated on the basis of the plastic part of the RO equation 1 in combination with the conversion in eq. 5.

$$\varepsilon_{plas} = \ln\left(1 + \left(\frac{\sigma}{K}\right)^{1/n}\right) \ . \tag{7}$$

Table 2 shows the median of the first calculated pairs of values.

Table 2 - Median pairs of values of modeled data

static data		**load release data**		**cyclic data**	
σ [MPa]	ε [%]	σ’ [MPa]	ε’ [%]	σ’’ [MPa]	ε’’ [%]
314.00	0	316.00	0	410.00	0
340.35	0.014	342.31	0.032	431.70	0.033
366.08	0.025	367.97	0.049	452.42	0.053
391.86	0.044	393.67	0.073	473.20	0.083
417.71	0.074	419.43	0.105	494.07	0.127
443.65	0.120	445.26	0.149	515.07	0.190
469.73	0.191	471.19	0.207	536.24	0.282
496.04	0.296	497.24	0.283	557.67	0.411
522.65	0.449	523.46	0.380	579.44	0.591
549.70	0.666	576.54	0.503	601.71	0.838

Obvious differences, especially between static and cyclic behavior, are evident. The approx. and the 0.2 % yield strength are distinctly increased. But the release behavior doesn't follow the static behavior either. Calculating the yield strength R_e', the following flow laws result, based on eq. 2:

$$f(\sigma, X)_{static} = F(\sigma - X) - 314 \tag{8}$$

$$f(\sigma, X)_{relief} = F(\sigma - X) - 316 \tag{9}$$

$$f(\sigma, X)_{cyclic} = F(\sigma - X) - 410. \tag{10}$$

Models 2 and 4 are based on a nonlinear kinematic Chaboche model (Lemaitre, 1990), which maps cyclic creeping and stress relaxation by a nonlinear evolution of the flow criterion.

Because it is a kinematic model, the flow surface moves with plastic deformation in the stress plane without changing the flow surface. However, there is a limitation, which restricts the displacement of the flow surface (Miramontes, 1996). The displacement of the flow surface is described with the kinematic hardening variable (khv) α. Eq. 11 shows the change of the khv. C and γ are the material characteristics of the Chaboche material model.

$$d\alpha = C\, d\varepsilon_p - \gamma\alpha\left|\varepsilon_p\right| \tag{11}$$

By integrating the change of the khv the following result is obtained:

$$\alpha = \nu\frac{C}{\gamma} + \left(\alpha_0 - \nu\frac{C}{\gamma}\right) \cdot e^{-(\varepsilon_p - \varepsilon_{p0})} \tag{12}$$

Stress is calculated with:

$$\sigma = \alpha + \nu T \tag{13}$$

Stress is described by equations 12 and 13 and depends on the current plastic strains ε_p and on the previous condition ε_{p0} and α_0, while the direction of motion is given by $\nu = \pm 1$. Analogous ε_{p0} and α_0 are equal to zero in case of first load behavior. Assuming an ideal adjustment of the khv to the real stress-strain curve, the constant T is set equal to the approx. yield stress R_e'.

$$T = R_e{}' \tag{14}$$

Finally, eq. 11-14 results in:

$$\sigma = \sum_{n=1}^{j} \alpha_j + \nu K = \sum_{n=1}^{j} \nu\frac{C_j}{\gamma_j} \cdot \left(1 - e^{-\gamma_j(\varepsilon_p)}\right) + \nu R_e{}' \tag{15}$$

The plastic area of the cyclic stress-strain curve can be divided into three areas, see fig. 4. A large slope is distinctive for area 1. Area 2 introduces the transition into a nearly flat and linear curve progression in area 3.

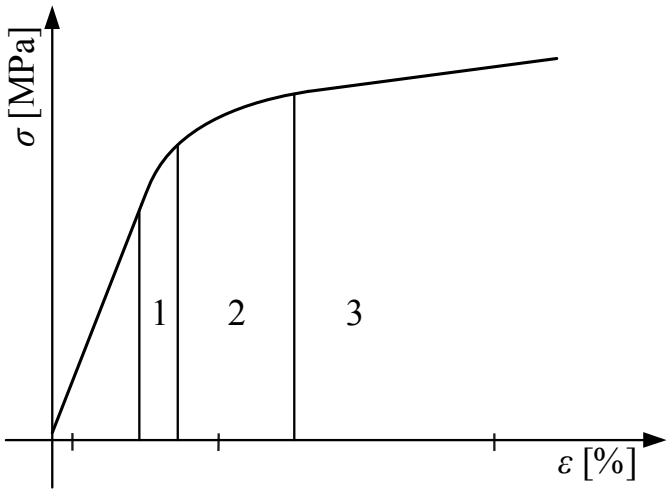

Fig. 4 Segmentation of cyclic stress-strain curve

According to (Lemaitre, 1990) a three times fragmented khv α is thus sufficiently accurate. The model parameters C_j and y_j are iteratively adapted to the cyclic stress-strain curve. C_1 corresponds to the slope of the curve after the yield strength, while γ_1 maps the fading hardening. In area 2 and 3, the transition to the nearly linear part of the curve is defined with $C_{2,3}$ and $\gamma_{2,3}$. The khv's are finally lifted to the corresponding stress level by means of the approximately determined yield strength R_e'. Table 3 lists the determined Chaboche model parameters. Similar to models 1 and 3, model 2 uses only the Chaboche material data at the beginning of the calculation. In model 4, hardening is applied in two stages similarly to model 3. The non-linear model is then calculated to estimate the influence of stress relaxation and creeping.

Table 3 - Chaboche model parameters

Parameter	Value
C_1	75885.8
γ_1	691.3
C_2	9789.7
γ_2	88.8
C_3	2058.6
γ_3	9.64
R_e'	410

VERIFICATION AND COMPARISON

A brake caliper of the KB-SfN GmbH, made of spheroidal graphite iron GJS 600-6 with an applied strain gauge on the strut, was tested with a constant load for comparative values, see fig. 5. Due to the bending of the strut, a 3-axle loading condition is developed. The strain gauge measures the strain in y- and x-direction, to verify the 2-axle surface load condition.

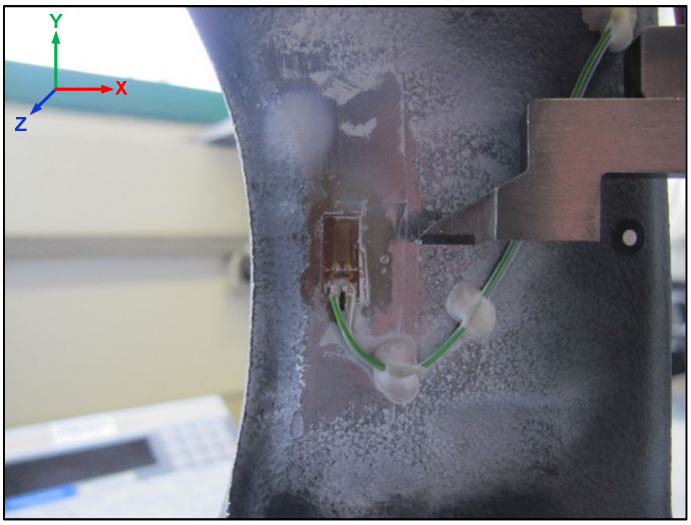

Fig. 5 - KB brake caliper with applied strain gauge

Table 1 shows median strain values of the individual models compared to the real data. During the first 20 load cycles, air pressure is adjusted to apply the nominal load, where significant plastic deformations already occur. The increase of the initial high plastic strains is already fading away in the subsequent 100 load cycles. Between the next 100 and 10,000 load cycles, plastic strain in y-direction only increases by approx. 88 µm/m. It can be concluded that the hardening of the material is so strong, that the stress amplitude can be beard almost completely elastically. Cyclic creeping could be responsible for the small increase in plastic strain at high load cycles.

Table 4 - Comparison of different material models

	cumulated plastic strain in y direction after x cycles [µm/m]					**computing time**	**cycles for computing time**
cycles	20	100	200	300	10.000	-	
real data	944	1114	1127	1142	1202	-	
model 1	523	523	523	523	523	≈ 10 min	2 cycles
model 2	544	569	582	596	-	≈ 9 h	300 cycles
model 3	1144	1144	1144	1144	1144	≈ 20 min	4 cycles
model 4	1169	1200	1207	1212	-	≈ 9h	300 cylces
	cumulated plastic strain in x direction after x cycles [µm/m]						
real data	-535	-624	-628	-636	-638		
model 1	-252	-252	-252	-252	-252		
model 2	-271	-285	-296	-305	-		
model 3	-631	-631	-631	-631	-631		
model 4	-653	-678	-691	-702	-		

Because of the high computing time, model 2 and 4 are cancelled after 300 cycles. The strains of the state of the art models 1 and 2 are too small due to the high initial material strength and thus do not give reliable data. The strains of model 1 and 3 remain the same, because the flow criterion is only changed twice discretely, and a new plasticizing doesn't occur after load step 1. Nevertheless model 3 is providing sufficiently high accuracies at a significantly lower computation time without the consideration of stress relaxation and creeping. Only during the first 20 load cycles the calculated strain is too high. This can be explained by adjustment of the pressure at the beginning of the test and therefore the allegedly smaller load. The real creep strain on the caliper can be approached very well with the two-stage hardening and the

subsequent non-linear material behavior in model 4. On the other hand, there is the enormous computing time since many load steps have to be calculated. Because the low creep strains are also not decisive for fatigue strength, they can be neglected for a damage calculation of materials with very pronounced hardening during the first load cycles.

In order to support this thesis, a damage calculation based on (Smith, 1970) is carried out according to eq. 16 for median values.

$$P_{SWT} = \sqrt{\sigma_o \cdot \varepsilon_t \cdot E} \tag{16}$$

$$\chi = \frac{1}{\sigma_{max}} \cdot \frac{d\sigma}{dx} \tag{17}$$

The damage calculations in fig. 6 show that only model 2 is able to represent a transient transition of hardening which is finished after 20 cycles. Hardening of all other models is finished after max. 3 cycles. In addition to the damage values, stress gradient effects in notches according to eq. 17 have to be considered for lifetime predictions (Siebel, 1955).

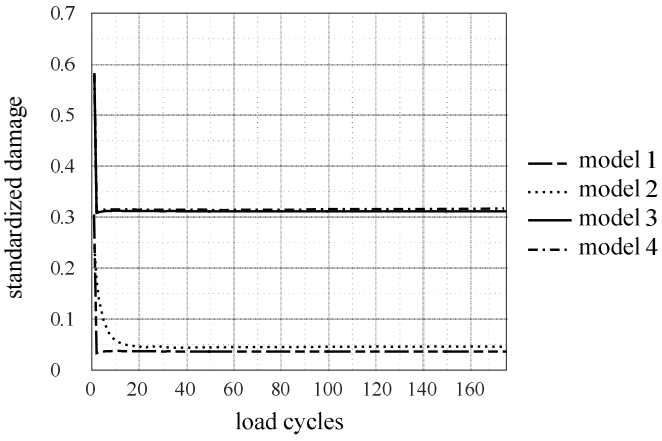

Fig. 6 - Damage calculation for the different material models

Fig. 7 shows damage and stress gradients of model 2 for different notch intensities based on eq. 16 and 17. Convergence already occurs very early too and this effect is reinforced with increasing notch intensity K_t. The amount of damage increases accordingly with increasing notch intensity. In addition the settling process is completed more quickly. This can be explained by the material behavior as follows:

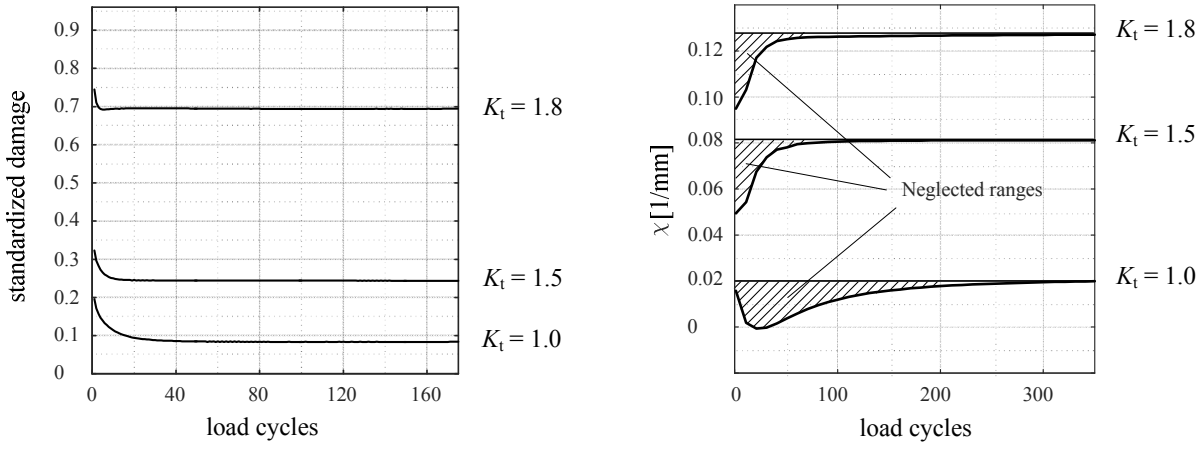

Fig. 7 - Damage and related stress gradient for different notch intensities

With increasing stress and thus increasing strain level, the increase in the khv α is flatter over the strain. This results in a large hardening at the beginning and an even faster stabilization of the material can be expected. Notches develop support effects that are included in the lifetime calculations by means of the related stress gradient (Siebel, 1955). Fig. 7 shows the course of the stress gradient at constant load amplitude. A settle process is identifiable, too.

Furthermore, the magnitude of the related stress gradient increases while the settling time decreases with increasing notch intensity. With a small notch effect, the course of the related stress gradient can change, because it does not only dependent on the notch shape, but also on the type of stress. The course of the stress gradient thus behaves very similar to the damage values. As a result, the error using model 3 decreases with increasing notch intensity. For a notch intensity of K_t = 1.8, the damage rate already stabilizes after approx. 6 load cycles and the gradient after approx. 50 load cycles. However, these observations are only based on simulation data so far and have to be verified with a detailed measurement.

With these investigations, it can be demonstrated, that time-dependent settling processes as well as cyclic creeping and stress relaxation can be neglected for fast hardening materials. The 3-step hardening model describes the 2-axle surface load condition in the caliper with sufficient accuracy and a low computation time.

STOCHASTIC MATERIAL MODELING AND LIFETIME CALCULATION

In case of casting iron materials in particular, fluctuating production processes and different chemical compositions of the castings sometimes result in considerable variance of the mechanical properties (Trubitz, 2004). For example, the copper content is essential for the shaping of the elongation at break. In order to take this variance into account for a lifetime calculation, Dazer (Dazer, 2016) proposed a stochastic lifetime calculation process, in which scattering of the input variables is considered.

The 3-step material model must therefore be capable of mapping the real scattering of the mechanical properties, which means that the stress-strain relationship has to be changed. Therefore, suitable scattering ranges of the parameters of the RO - equation have to be determined. In the first step, the variance of the respective 0.2 % - yield strength and the tensile strength of the material batches is used.

Fig. 8 shows the variance ranges of material properties for initial loading. All of them follow a Weibull distribution. The elastic part is completely defined by the variance of the Young's modulus. For the elastic-plastic range, the 0.2 % - yield strength and the tensile strength provide two supporting points of the Ramberg-Osgood equation. The 0.2 % - yield strength is always assigned to a plastic strain of $\varepsilon = 0.2\,\%$, see eq. 18, while the tensile strength is assigned to the uniform elongation ε_G, see eq. 19.

Using Monte-Carlo sampling with 10.000 iterations the result is a one-dimensional range of variation for supporting point 1 and a two-dimensional range of variation for supporting point 2, because uniform elongation is also scattering. Correlation between tensile strength and 0.2 % yield strength of the measured data is nearly linear and was taken into account. An obvious correlation between tensile strength and uniform elongation could not be demonstrated with the measured data.

Fig. 9 shows the procedure with the associated point clouds of the supporting points as well as the median, the min. and the max. Ramberg-Osgood curve for initial loading. The range of variance for initial release and cyclic data are determined analogously, with the difference that

another stress level is selected for support point 2, because the tensile strength is not directly measurable in strain-controlled fatigue tests. In this case, also a one-dimensional range of variance results for support point 2, since the tension is measured at a defined elongation.

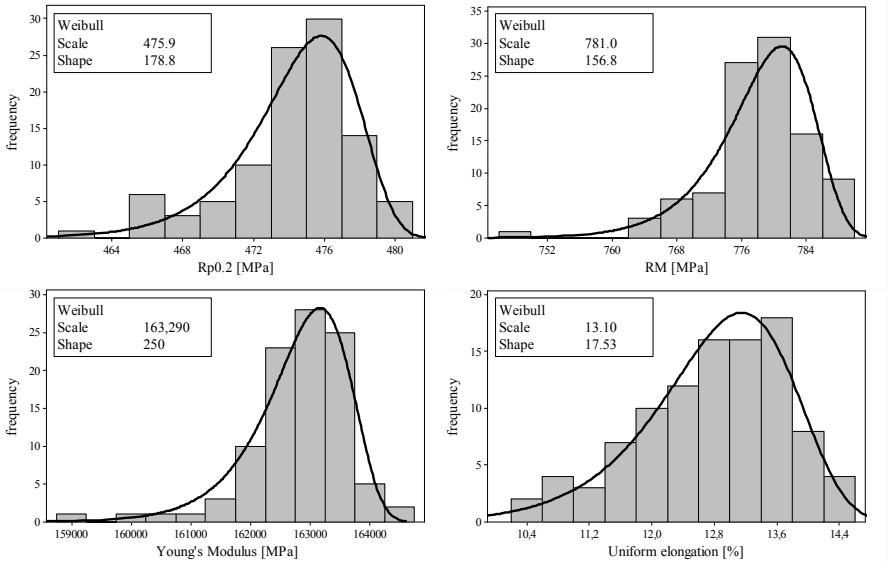

Fig. 8 - Variance of material properties

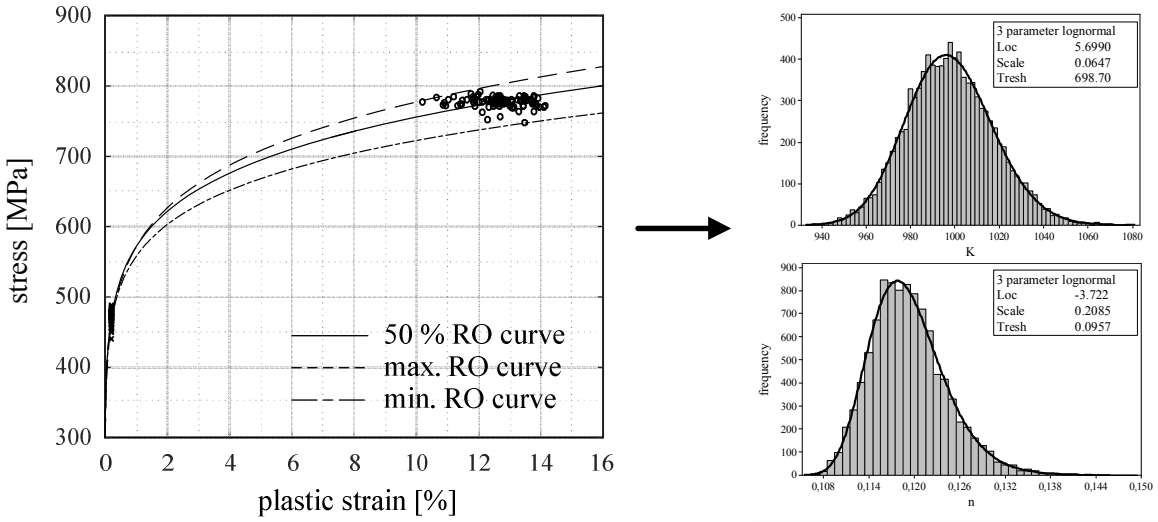

Fig. 9 - Monte-Carlo procedure for variance determination of RO parameters

$$\varepsilon_{plas_1} = \left(\frac{\sigma_1}{K}\right)^{1/n} \Rightarrow 0.002 = \left(\frac{R_{p0.2}}{K}\right)^{1/n} \tag{18}$$

$$\varepsilon_{plas_2} = \left(\frac{\sigma_2}{K}\right)^{1/n} \Rightarrow \varepsilon_G = \left(\frac{R_m}{K}\right)^{1/n} \tag{19}$$

Executing the procedure with 10,000 Monte-Carlo iterations result in the probability functions of the RO parameter of static, release and cyclic data.

With the determined variance of the parameters and the probability functions, it is now possible to represent scattering loading conditions in the caliper like in reality, e.g. by batch fluctuations. The advantage of this method is the enormous flexibility and adaptability of the stochastic model. Due to the integration with pairs of values according to eq. 6 and 7, the new yield strengths, the associated pairs of values for stress and strain and the corresponding flow criteria according to eq. 8-10 are obtained directly in case of changes in the material parameters.

According to (Zahavi, 1996) the level of cyclical hardening is highly depend on the metal production process. The production process again is dependent on many random variables like casting temperature and chemical composition. Therefore it is not possible to demonstrate a generally valid correlation between static, release and cyclic material behavior. For that reason, differently pronounced hardening effects have to be taken into account. Hence, the individual curves (static, release, cyclic data) are modeled independently, which means that a higher static yield strength does not automatically mean an equally higher cyclic yield strength. This makes it possible to map different phenomena of material behavior, such as the following limiting cases:

- Initially weak materials with weak hardening,
- Initially strong materials with strong hardening,

but also:

- Initially weak materials with strong hardening,
- Initially strong materials with weak hardening.

The stochastic lifetime calculations proposed by (Dazer, 2016) can be carried out using the defined material behavior. The results are shown in fig. 10 for different calipers with different notch intensities at the location of failure. The calculations result in an entire mapped virtual Weibull distribution, which approximates the real data with a high accuracy. In addition, the accuracy increases with increasing notch intensity, which can be ascribed to the smaller calculation error from the settling process. Certainly, the error with small notch intensities could also be explained with the smaller sample sizes of the real data.

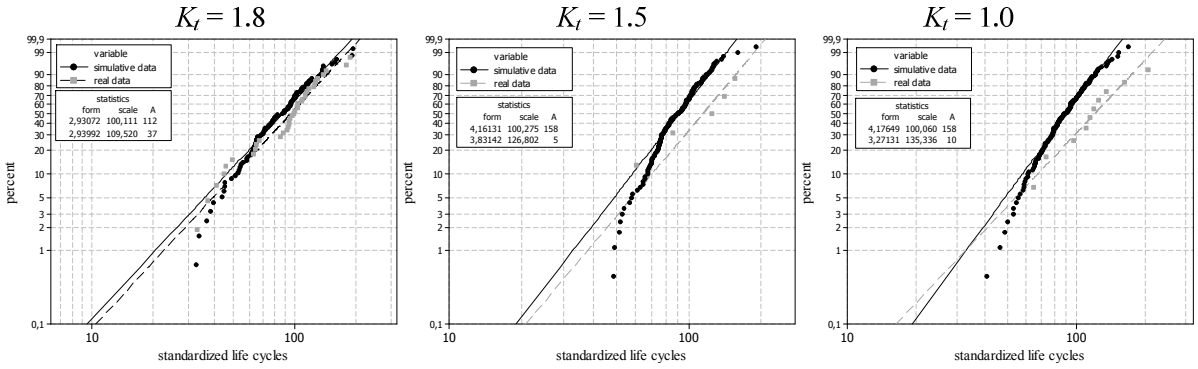

Fig. 10 - Stochastic lifetime calculation according to (Dazer, 2016) for different notch intensities

SUMMARY

In the first part of this work was shown, that a very good approximation of the material behavior of cyclically hardening materials can be achieved with a 3-step transition from static to cyclic behavior. For GJS 600, the transient settling process is already finished between 20 and 100 load cycles depending on the notch intensity. Thus the neglected damage-relevant regions are very small. In summary, it can be revealed, that the time-dependent effects and

settling processes for the material description can be neglected for hardening materials with weakly pronounced creeping behavior.

For the stochastic lifetime calculations according to (Dazer, 2016), the 3-stage mkh material model is stochastically described in the second part of this work. This allows mapping of strong and weak hardening behavior with analogous initial conditions, making the model very flexible to use. The empirical validation due to the lifetime calculations of the brake calipers shows that the material model maps the real loading conditions with very high accuracy.

REFERENCES

[1]-Nelson, W.: Accelerated Testing: Statistical Models, Test Plans, and Data Analysis. New Jersey: John Wiley & Sons, 2004

[2]-Berns, H.; Theisen, W.: Eisenwerkstoffe. Berlin Heidelberg: Springer Verlag, 2013, p. 180

[3]-Dazer, M.; et al.: Optimale Lebensdauertestplanung durch Berücksichtigung von Vorkenntnissen aus stochastischen Betriebsfestigkeitssimulationen. Düsseldorf: VDI Verlag GmbH, VDI-Berichte 2279, 18. SIMVEC Conference 2016, 2016, p. 777-788

[4]-Haibach, E.: Betriebsfestigkeit: Verfahren und Daten zur Bauteilberechnung. Berlin Heidelberg: Springer Verlag, 2006, p. 343-344

[5]-Lemaitre, J.; Chaboche, J.: Mechanics of solid materials. Cambridge: Cambridge University Press, 1990, p. 218-222

[6]-Leutwein, H.: Einfluss von Autofrettage auf die Schwingfestigkeit innendruckbelasteter Bauteile aus Kugelgraphitguss. Illmenau, 2007, p. 38, p. 49-52

[7]-Miramontes, D.; Merabet, O.: Reynouard J.: Kinematic hardening model based on general plasticity for RC structures. Paper No. 483, Amsterdam: Elsevier Science Ltd, 1996

[8]-Osgood, W.; Ramberg W.: Description of StressStrain Curves by Three Parameters. Washington DC: National Bureau of Standards, NACA Technical Note 902, 1943

[9]-Prager, W.: The theory of plasticity - a survey of recent achievements. London: Proceedings of the Institution of Mechanical Engineers, Vol. 169, 1955, p. 41-57

[10]-Roos, E.; Maile, K.: Werkstoffkunde für Ingenieure. 5. Auflage, Berlin Heidelberg: Springer Vieweg, 2015, p. 72-90

[11]-Schneider, R.: Örtliche Bewertung der Schwingfestigkeit von Gewindeverbindungen. Darmstadt, 2011. p. 24

[12]-Beanspruchung. Düsseldorf: VDI-Z. 97 Nr. 5., 1955, S. 121-126

[13]-Smith, K.; Watson P.; Topper, T.: A stress-strain function for the fatigue of metals. Band 5, Pennsylvania, ASTM Journal of Materials, 1970, p. 767-778

[14]-Trubitz, P.; Rehmer, B.; Pusch, G.: Die Ermittlung elastischer Konstanten von Gusseisenwerkstoffen. Frankfurt: Werkstoff-Informationsgesellschaft mbH, 2004, p. 267-272

[15]-Zahavi, E.; Torbilo, V.: Fatigue design: Life expectancy of machine parts. Boca Raton: CRC Press, 1996.